Investigation of one-dimensional photonic bandgap structures containing lossy double-negative metamaterials through the Bloch impedance

Fenghua Shi,[1] Yihang Chen,[1,2,*] Peng Han,[1,4] and Costas M. Soukoulis[2,3]

[1]*Laboratory of Quantum Information Technology, School of Physics and Telecommunication Engineering, South China Normal University, Guangzhou 510006, China*
[2]*Ames Laboratory and Department of Physics and Astronomy, Iowa State University, Ames, Iowa 50011, USA*
[3]*Institute of Electronic Structure and Lasers (IESL), FORTH, Heraklion, Crete 71110, Greece*
[4]*e-mail: hanp@scnu.edu.cn*
**Corresponding author: chenyh@ameslab.gov*

Received March 1, 2013; accepted March 27, 2013;
posted April 10, 2013 (Doc. ID 186230); published May 6, 2013

The Bloch impedance is studied and used to understand the properties of the absorption loss in one-dimensional photonic crystals (PCs) composed of air and metal-based double-negative metamaterials. We find that as the frequency increases across the zero-$\bar{n}$ gap of the considered structures, the modulus of the Bloch impedance always decreases from a maximum to a minimum value. On the other hand, the frequency dependence of the phase angle of the Bloch impedance is greatly influenced by the ratio of the electric to the magnetic damping coefficient γ_e/γ_m of the metamaterials. When the phase angle of the Bloch impedance reaches maximum inside the zero-$\bar{n}$ gap, the impedance mismatch between the incident medium and the considered PC becomes greatest, the reflection will be strongest and a minimum absorption will be observed. As γ_e/γ_m increases, the frequency corresponding to the minimum absorption shifts from the lower to the upper gap edge. We also show that the main characteristics of both the Bloch impedance and the absorption loss are insensitive to the geometrical parameters. Our study offers a valuable reference in the designs of zero-$\bar{n}$ gap with optimized properties.

OCIS codes: (260.2110) Electromagnetic optics; (050.5298) Photonic crystals; (160.3918) Metamaterials.
http://dx.doi.org/10.1364/JOSAB.30.001473

1. INTRODUCTION

Photonic crystals (PCs) [1–3], a type of artificial composites, have attracted much interest in the last two decades because of their potential ability to control the motion of photons in a similar way as the semiconductor crystals affect the motion of electrons. Conventional PCs are composed of periodic dielectric or metallo-dielectric nanostructures in which photonic bandgaps (PBGs) exist due to the interference of multiple Bragg scattering. Potential applications of the PCs have been proposed in scientific and technical areas, such as filters [4], optical switches [5], and suppression of spontaneous emission [6]. However, such applications are substantially limited since the electromagnetic (EM) properties of the Bragg gaps strongly depend on the lattice constant, incident angle, and disorder.

A possible way to overcome such limitations is to introduce metamaterials with negative refractive indices into the PC structure. The so-called negative-index or double-negative (DNG) metamaterials, possessing simultaneously negative permittivity ε and negative permeability μ [7], have attracted a great deal of attention since their first experimental realization in 2001 [8,9]. It has been demonstrated that stacking alternating layers of ordinary double-positive (DPS) materials (with positive ε and positive μ) and DNG metamaterials can lead to a special type of PBG when the volume averaged effective refractive index ($\bar{n}$) equals zero [10]. Such a PBG, named the zero-$\bar{n}$ gap, originates from the Bragg scattering, possesses properties different from the traditional Bragg PBGs. The zero-$\bar{n}$ gap has weak dependence on the lattice constant and disorder [10,11], can be designed to be insensitive to the incident angle [12,13].

For DNG metamaterials, negative permeability is the result of a strong resonant response to an external magnetic field while negative permittivity appears by either a plasmonic or a resonant response to an external electric field. Several types of designs were proposed to realize both electric and magnetic responses simultaneously, for example, split ring resonators combined with thin wires [8,9], cut wire pairs, and fishnet structures [14–16]. These artificial materials are designed based on the metallic structures, in which absorption loss is inevitable. Such losses have great effect on the properties of the DNG metamaterials, which may eventually influence the EM properties of the zero-$\bar{n}$ gap. Therefore, it is necessary to investigate the properties of the zero-$\bar{n}$ gap when absorption loss is considered. It should be noticed that there may exist a great difference of the absorption between the electric and the magnetic field components of the wave propagating through the DNG metamaterials. On the other hand, as the frequency varies, the EM field distribution inside the

PC changes significantly, which may lead to large changes of the absorption loss. Considering the above factors, the Bloch impedance, determined by the electric and the magnetic field distributions inside the periodic structure, is used to understand and predict the characteristics of the absorption loss.

In this paper, we investigate the main features of the Bloch impedance inside the multilayered structure combining DPS and DNG materials when losses are taken into account. We discuss the relationship between the properties of the Bloch impedance and those of the absorption loss. The discussions are organized as follows. In Section 2, we introduce the theoretical methods. In Section 3, we discuss the Bloch impedance and its relevance to the absorption loss of the considered system. In Section 4, we investigate the influence of the structural parameters on the Bloch impedance and the absorption loss inside the zero-$\bar{n}$ gap. Finally, our conclusions are presented in Section 5.

2. MODEL AND NUMERICAL METHODS

Consider a one-dimensional PC consisting of alternating layers of DPS and DNG materials, as shown in Fig. 1. Layers 1 and 2 represent the DPS and DNG material layers with the thicknesses of d_1 and d_2, respectively. $d = d_1 + d_2$ is the lattice constant. In this paper, we choose air as the DPS material with $\varepsilon_1 = 1$, $\mu_1 = 1$. The DNG materials are considered to be realized from metal-based metamaterial. The dispersion of such metal-based metamaterials can be described by the Drude model [11,17,18], that is,

$$\varepsilon_2(\omega) = \varepsilon_0 - \frac{\omega_{\mathrm{ep}}^2}{\omega(\omega + i\gamma_e)}, \tag{1}$$

$$\mu_2(\omega) = \mu_0 - \frac{\omega_{\mathrm{mp}}^2}{\omega(\omega + i\gamma_m)}, \tag{2}$$

where ω_{ep} and ω_{mp} correspond to the electronic plasma frequency and magnetic plasma frequency. γ_e and γ_m denote the electric and magnetic damping coefficients that contribute to the absorption loss. ω is the angular frequency measured in gigahertz. In the following calculations, we choose $\omega_{\mathrm{ep}} = \omega_{\mathrm{mp}} = 10$ GHz, $\varepsilon_0 = 1.21$, $\mu_0 = 1$.

We assume that the layers of the considered PC are oriented in the *yoz* plane, as shown in Fig. 1. Let a plane EM wave propagating in the $+z$ direction be incident normally on the boundary $z = 0$ from free space into the periodic structure.

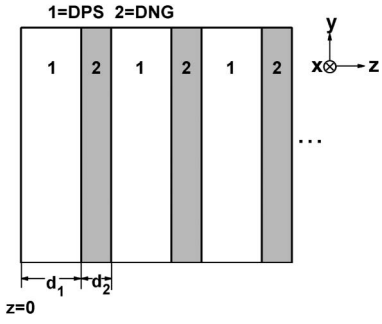

Fig. 1. Schematic representation of the DPS/DNG multilayered structure.

The electric and magnetic fields of adjacent layers can be related via a transfer matrix [19–21]

$$M_j = \begin{bmatrix} \cos(k_j d_j) & i/q_j \sin(k_j d_j) \\ iq_j \sin(k_j d_j) & \cos(k_j d_j) \end{bmatrix}, \tag{3}$$

where $k_j = \omega\sqrt{\varepsilon_j}\sqrt{\mu_j}$ and $q_j = \sqrt{\mu_j}/\sqrt{\varepsilon_j}$ $(j = 1, 2)$.

The transfer matrix of a unit cell of the PC can be obtained as

$$M = M_1 M_2 = \begin{bmatrix} u_{11} & u_{12} \\ u_{21} & u_{22} \end{bmatrix}, \tag{4}$$

where u_{ij} $(i, j = 1, 2)$ is the matrix element. The relationship between the EM fields at $z = nd$ $(n = 0, 1, 2, 3, \ldots)$ and those at $z = (n + 1)d$ can be written as

$$\begin{bmatrix} E_n \\ H_n \end{bmatrix} = \begin{bmatrix} u_{11} & u_{12} \\ u_{21} & u_{22} \end{bmatrix} \begin{bmatrix} E_{n+1} \\ H_{n+1} \end{bmatrix}. \tag{5}$$

According to Bloch's theorem [22,23], we have

$$\begin{bmatrix} u_{11} - e^{-iK_B d} & u_{12} \\ u_{21} & u_{22} - e^{-iK_B d} \end{bmatrix} \begin{bmatrix} E_{n+1} \\ H_{n+1} \end{bmatrix} = 0, \tag{6}$$

where K_B is the Bloch wave vector. Then the dispersion relation of the PC can be obtained by solving [24]

$$\cos(K_B d) = (u_{11} + u_{22})/2. \tag{7}$$

From Eq. (6), the phase coefficient $e^{-iK_B d}$ can also be solved and written as

$$e^{-iK_B d} = \frac{(u_{11} + u_{22}) \pm \sqrt{(u_{11} + u_{22})^2 - 4}}{2}. \tag{8}$$

The Bloch impedance is defined as

$$Z_B = \frac{E_{n+1}}{H_{n+1}} Z_0. \tag{9}$$

Combining Eq. (6), we have

$$Z_B = -\frac{u_{12}}{u_{11} - e^{-iK_B d}} Z_0. \tag{10}$$

By Substituting Eq. (8) into Eq. (10), we can obtain the expression

$$Z_B = \frac{\pm 2u_{12}}{u_{11} - u_{22} + \sqrt{(u_{11} + u_{22})^2 - 4}} Z_0. \tag{11}$$

According to the Fresnel reflectance equation, the reflectance of a semi-infinite PC can be written as

$$R = \left| \frac{1 - Z_B/Z_0}{1 + Z_B/Z_0} \right|^2, \tag{12}$$

where Z_0 is the intrinsic impedance of the incident medium.

In lossless cases, the solutions of Bloch wave vector K_B in Eq. (6) determine the band structure of the considered PC with allowed zones separated by bandgaps. Real solution

for K_B can be found at frequencies within the allowed bands. If the frequency of the wave locates inside a forbidden gap, K_B becomes pure imaginary and R equals to 1. In fact, the band structure of PCs can also be obtained from Bloch impedance in lossless situations [25,26]. In these cases, Bloch impedance Z_B is complex within the passband while it becomes pure imaginary inside the bandgap. However, when losses are taken into account, the real and imaginary parts of K_B and Z_B will both be nonzero.

3. BLOCH IMPEDANCE AND ITS RELEVANCE TO ABSORPTION LOSS

Impedance has been applied in reducing the insertion loss for traditional waveguides and transmission lines. Investigations of the impedance are also helpful for understanding the process of the energy flow for wave propagating from one medium to another. Similarly, the Bloch impedance, as an intrinsic characteristic of the PC, can be used to improve the performance of the PC waveguides by reducing their insertion losses [26–28]. However, the Bloch impedance has attracted much less attention than the Bloch wave vector. Here, we will investigate the properties of the Bloch impedance of the considered DPS/DNG PC. The relationship between the absorption loss and the Bloch impedance will also be discussed.

In Fig. 2, we plot the average refractive index $\bar{n}$, Bloch wave vector K_B, the complex modulus $|Z_B|$, and the phase angle θ_{ZB} of the Bloch impedance versus the frequency for an infinite DPS/DNG periodic structure without considering the absorption loss ($\gamma_e = \gamma_m = 0$). It was pointed out that the zero-$\bar{n}$ gap opens from a frequency where the volume averaged index $\bar{n} = (1/d)\int_0^d n(z)\mathrm{d}z$ equals to zero [10]. For lossy structures, the zero-$\bar{n}$ gap should originate from frequency where $(1/d)\int_0^d \mathrm{Re}(n(z))\mathrm{d}z = 0$. As shown in Fig. 2(a), $\bar{n} = 0$ is satisfied at 7.867 GHz, from which a PBG emerges. Such a zero-$\bar{n}$ gap exists in frequency range from 7.651 to 8.164 GHz, in which K_B is pure imaginary, as shown in Fig. 2(b). On the other hand, the Bloch impedance Z_B calculated from Eq. (11) is pure imaginary within the zero-$\bar{n}$ gap and is complex inside the passbands, as show in Fig. 2(c).

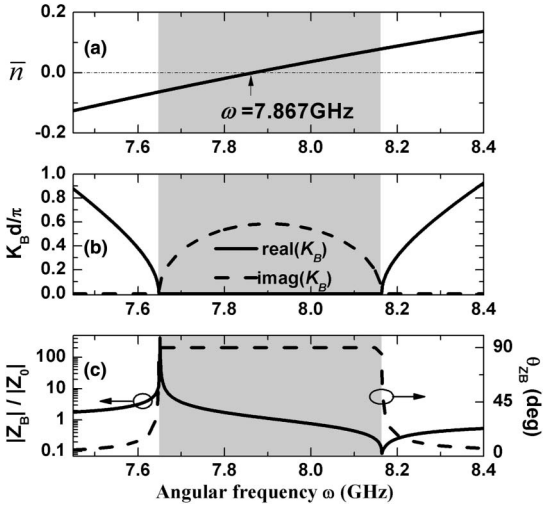

Fig. 2. (a) $\bar{n}$, (b) K_B, and (c) $|Z_B|$ and θ_{ZB} as a function of the angular frequency ω in infinite DPS/DNG PC with $d_1 = 6$ mm, $d_2 = 12$ mm, and $\gamma_e = \gamma_m = 0$. The gray areas correspond to the zero-$\bar{n}$ gap.

We focus on the frequency range corresponding to the zero-$\bar{n}$ gap. It can be seen that, as the frequency increases across the zero-$\bar{n}$ gap, the value of $|Z_B|/|Z_0|$ decreases, which means that the electric field component becomes weaker while the magnetic field component becomes stronger. For a more clear understanding, the electric and magnetic field distributions inside a 100-period DPS/DNG PC at $\omega = 7.68$ GHz and $\omega = 8.14$ GHz are simulated and shown in Figs. 3(a) and 3(b). As shown in Fig. 3(a), the relative amplitude of the electric field $|E_r|(= |E|/|E_{\mathrm{in}}|$, E_{in} is the electric field amplitude of the incident wave) is much larger than that of the magnetic field $|H_r|(= |H|/|H_{\mathrm{in}}|$, H_{in} is the magnetic field amplitude of the incident wave) at 7.68 GHz where a large value of $|Z_B|$ exhibits in Fig. 2(c). On the other hand, as shown in Fig. 3(b), the relative amplitude of the magnetic field is much larger than that of the electric field at 8.14 GHz where $|Z_B|/|Z_0|$ is much smaller than 1. Such differences of the electric and magnetic field distributions between different frequencies are due to the changes of the interference of the scattering inside the PC structure.

Furthermore, as shown in Fig. 2(c), θ_{ZB} keeps a fixed value of $\pi/2$ in the bandgap. Therefore, according to the definition of energy flux $S = |E|^2 \cos(\theta_{ZB})/(|Z_B|/|Z_0|)$, the energy flux will be zero and a complete reflection of the wave energy appears. In fact, both $|Z_B|$ and θ_{ZB} are closely associated with the reflection from PCs. If Z_B equals Z_0, i.e., a perfect impedance match between the incident medium (free space) and the considered PC, a perfect transmission will be observed and the reflectance will become zero. On the other hand, as $|Z_B|/|Z_0|$ deviates from 1 or θ_{ZB} deviates from 0°, the greater the impedance mismatch, the larger the reflectance will be. When Z_B becomes pure imaginary, a complete impedance mismatch occurs, the wave cannot propagate forward and the reflectance becomes 1, which corresponds to the case in a gap.

When absorption is taken into account, the reflectance of the PC can still be obtained via the Bloch impedance by using Eq. (12). Here, we try to find out the relationship between the absorption of the PC and the Bloch impedance. For an infinite lossy PC structure, the transmittance is zero, the absorptance can be obtained from

$$A = 1 - R = 1 - \left|\frac{1 - Z_B/Z_0}{1 + Z_B/Z_0}\right|^2. \tag{13}$$

Using Eq. (13), the dependence of the absorption on Z_B is calculated and plotted in Fig. 4. It can be seen from Fig. 4 that,

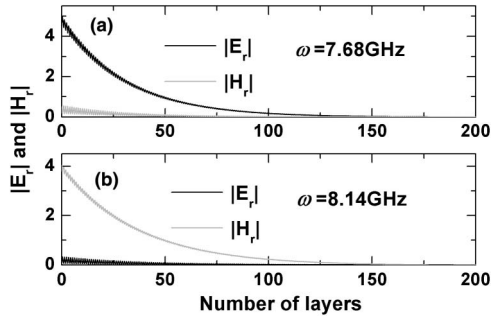

Fig. 3. EM field distributions in lossless DPS/DNG PC with $d_1 = 6$ mm, and $d_2 = 12$ mm at (a) $\omega = 7.68$ GHz and (b) $\omega = 8.14$ GHz near the lower and upper gap edge, respectively.

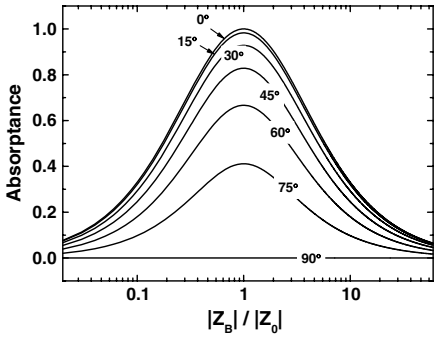

Fig. 4. Dependence of absorptance on $|Z_B|$ under different values of θ_{ZB}.

as $|Z_B|$ deviates from $|Z_0|$ or θ_{ZB} increases, the absorptance decreases. This can be understood as the greater impedance mismatch leads to the larger reflection and the smaller absorption. On the other hand, when the impedance of the incident space and that of the considered PC are well matched, i.e., Z_B equals to Z_0, most EM energy will transmit into the PC and finally be absorbed by DNG materials, the absorption of the considered system becomes maximum. As shown in Fig. 4, when $|Z_B|/|Z_0|$ is close to 1, the absorptance becomes insensitive to the changes of $|Z_B|$. We can also see that the absorptance becomes quite sensitive to θ_{ZB} when $|Z_B| \to |Z_0|$ and θ_{ZB} is large. Such results, attributed to the difference between the influence of $|Z_B|$ and that of θ_{ZB} on the impedance mismatch, are useful for understanding the properties of the absorption loss in the DPS/DNG PC.

4. INFLUENCE OF THE STRUCTURE PARAMETERS ON BLOCH IMPEDANCE AND ABSORPTION LOSS

In this section, we will investigate how the structural parameters of the DPS/DNG PC influence the Bloch impedance and the corresponding absorption. In Fig. 5, we plot $|Z_B|$, θ_{ZB} and the absorptance versus the frequency for the DPS/DNG PC under different damping coefficients: (a) and (b) $\gamma_e/\gamma_m = 10$; (c) and (d) $\gamma_e/\gamma_m = 1$; (e) and (f) $\gamma_e/\gamma_m = 0.1$. It can be seen that, for all cases, the Bloch impedance are complex numbers, $|Z_B|$ decreases from a maximum to a minimum value as the frequency increases across the zero-$\bar{n}$ gap.

We focus on the case with $\gamma_e/\gamma_m = 10$, where the electric damping is more pronounced than the magnetic damping. As shown in Fig. 5(a), at frequencies near the lower edge of the zero-$\bar{n}$ gap, $|Z_B|$ has a large value, meaning that the relative amplitude $|E_r|$ is much larger than $|H_r|$. Combining with a larger absorption for the electric field component of the wave (because $\gamma_e > \gamma_m$) propagating through the DNG metamaterial, it can be expected that relative large absorption appears in frequency range near the lower gap edge, which is verified in Fig. 5(b). On the other hand, we can see from Fig. 5(a) that, as the frequency increases inside the zero-$\bar{n}$ gap from 7.65 to 8.16 GHz, $|Z_B|/|Z_0|$ decreases from 2.2 to 0.5. θ_{ZB} is close to 90° at frequencies near the upper gap edge. As discussed in the last section, the absorption is sensitive to θ_{ZB} rather than $|Z_B|$ when $|Z_B| \to |Z_0|$ and $\theta_{ZB} \to 90°$. In this case, the absorption inside zero-$\bar{n}$ gap is mainly determined by θ_{ZB}. As shown in Fig. 5(b), within the zero-$\bar{n}$ gap, as θ_{ZB} increases, greater impedance mismatch occurs, the reflection becomes larger

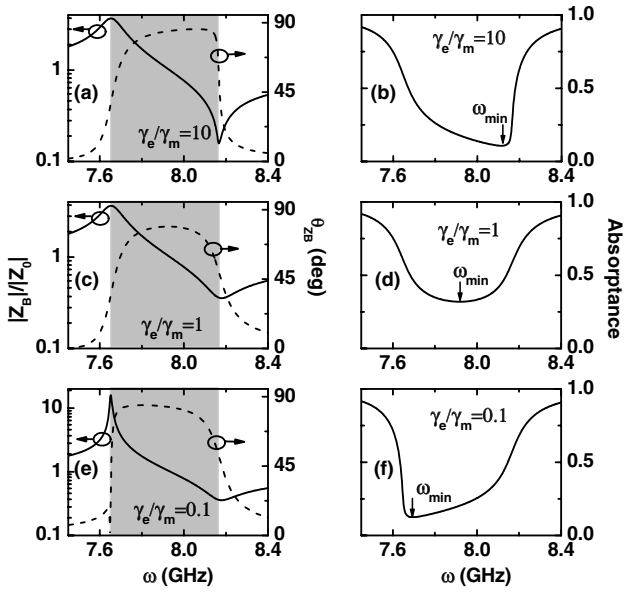

Fig. 5. $|Z_B|$, θ_{ZB} and absorptance versus frequency in DPS/DNG PC under different values of γ_e/γ_m: (a) and (b) $\gamma_e/\gamma_m = 10$ with $\gamma_e = 0.01$ GHz, $\gamma_m = 0.001$ GHz; (c) and (d) $\gamma_e/\gamma_m = 1$ with $\gamma_e = 0.01$ GHz, $\gamma_m = 0.01$ GHz; and (e) and (f) $\gamma_e/\gamma_m = 0.1$ with $\gamma_e = 0.001$ GHz, $\gamma_m = 0.01$ GHz. The thicknesses of the layers are $d_1 = 6$ mm and $d_2 = 12$ mm. The gray areas represent the zero-$\bar{n}$ gap.

and the absorption becomes smaller. Such result is in accordance with that in Fig. 4. Similarly, the relationship between the properties of Z_B and those of absorption loss inside the zero-$\bar{n}$ gap can be analyzed when γ_e/γ_m is changed, as shown from Figs. 5(c) to 5(f).

It can be also seen from Fig. 5 that, θ_{ZB} reaches maximum at a frequency $\omega_{\min}$ inside the zero-$\bar{n}$ gap, where a minimum absorptance can therefore be found. As γ_e/γ_m varies, the frequency dependence of θ_{ZB} changes, hence $\omega_{\min}$ changes as well. The dependence of $\omega_{\min}$ on γ_e/γ_m was investigated and shown in Fig. 6. It can be seen that $\omega_{\min}$ moves from the lower to the upper gap edge as γ_e/γ_m increases from 0.01 to 100. Such results are helpful for predicting when low absorption loss takes place inside the zero-$\bar{n}$ gap of the lossy PC structure.

Next, we investigate the dependences of the impedance and the absorption on γ_m when γ_e/γ_m is fixed. Taking $\gamma_e/\gamma_m = 1$

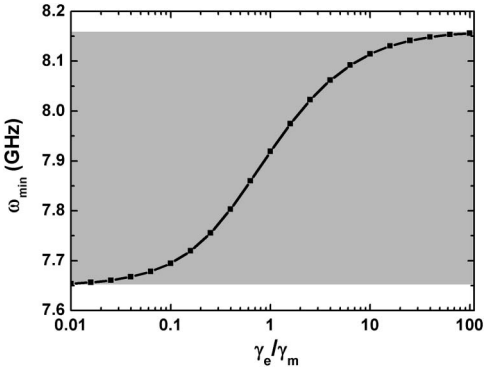

Fig. 6. $\omega_{\min}$ as a function of γ_e/γ_m when γ_m is fixed to be 0.001 GHz. The gray area corresponds to the zero-$\bar{n}$ gap. The thicknesses of the layers are $d_1 = 6$ mm and $d_2 = 12$ mm.

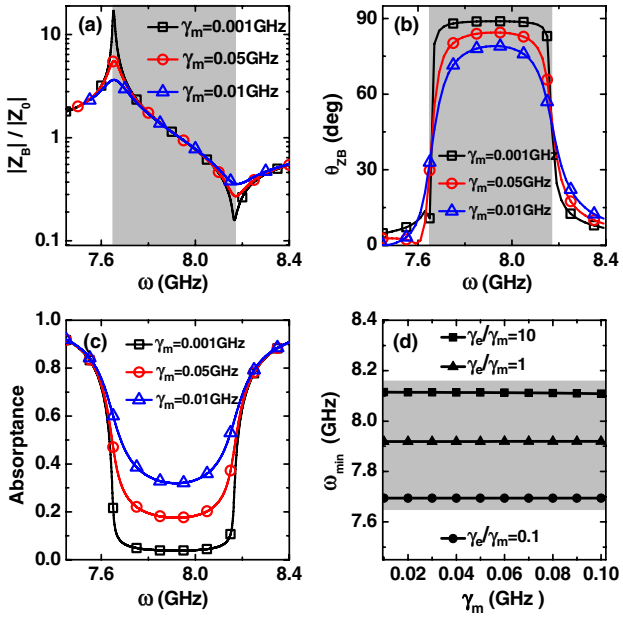

Fig. 7. (a) $|Z_B|$, (b) θ_{ZB}, and (c) absorptance versus ω under different γ_m in DPS/DNG PC with $\gamma_e/\gamma_m = 1$. (d) $\omega_{\min}$ as a function of γ_m under different values of γ_e/γ_m. The thicknesses of the layers are $d_1 = 6$ mm and $d_2 = 12$ mm. The gray area corresponds to the zero-$\bar{n}$ gap.

for instance, in Fig. 7 we plot $|Z_B|$, θ_{ZB} and absorptance versus angular frequency under different γ_m. As shown in Fig. 7(a), the values of $|Z_B|$ corresponding to different γ_m are almost the same in the central region of the zero-$\bar{n}$ gap, evident differences can only be found near the gap edges. On the other hand, it can be seen from Fig. 7(b) that θ_{ZB} decreases significantly as γ_m increases, meaning that the impedance mismatch of the considered system weakens, more energy can transmit into the PC structure and eventually be absorbed. Hence, the absorption becomes larger as γ_m increases, as shown in Fig. 7(c). It can also be observed from Fig. 7(b) that, for different values of γ_m, θ_{ZB} reaches maximum at almost the same frequency. Such a result causes $\omega_{\min}$ to remain almost unchanged as γ_m varies, as shown in Fig. 7(c). In Fig. 7(d), we show the dependence of $\omega_{\min}$ on γ_m under different values of γ_e/γ_m. We can observe that $\omega_{\min}$ is independent of γ_m when γ_e/γ_m is fixed.

Then we proceed to figure out how the geometrical parameters affect the Bloch impedance and the absorption loss. In Fig. 8, we plot $|Z_B|$, θ_{ZB} and the absorptance versus angular frequency under different d_1 in PC structure with $d_1/d_2 = 1/2$ and $\gamma_e = \gamma_m = 0.001$ GHz. It can be seen that $|Z_B|$ and θ_{ZB} are both insensitive to d_1, hence both the frequency range of the zero-$\bar{n}$ gap and the corresponding absorption remain invariant. The dependence of $\omega_{\min}$ on d_1 is investigated and shown in Fig. 8(d). It is seen that $\omega_{\min}$ remains constant as d_1 varies when γ_e/γ_m is fixed.

Next, we change the thickness ratio d_1/d_2 and study the Bloch impedance and the absorption loss of the considered system. In Fig. 9, we plot $|Z_B|$, θ_{ZB} and absorptance as a function of angular frequency in PC structure with different d_1/d_2. Here, we choose $d_1 = 6$ mm, $\gamma_e = 0.01$ GHz and $\gamma_m = 0.001$ GHz. It can seen that as d_1/d_2 increases, there is a redshift of the curve of $|Z_B|$, meaning that the zero-$\bar{n}$ gap will shift to lower frequencies as well. Furthermore, for different values of d_1/d_2, the properties of $|Z_B|$ and θ_{ZB} are similar. As ω increases across the zero-$\bar{n}$ gap, $|Z_B|$ decreases, θ_{ZB} increases and reaches maximum near the higher gap edge. Therefore, $\omega_{\min}$, corresponding to the minimum absorption, also appears near the upper gap edge for all three cases, as shown in Fig. 9(c). Figure 9(d) shows $\omega_{\min}$ as a function of d_1/d_2 in PC structure with $d_1 = 6$ mm. It can seen that although the zero-$\bar{n}$ gap and $\omega_{\min}$ change significantly as d_1/d_2 varies, the relative position of $\omega_{\min}$ inside the bandgap remains invariant. From the results shown in Figs. 8 and 9, we can

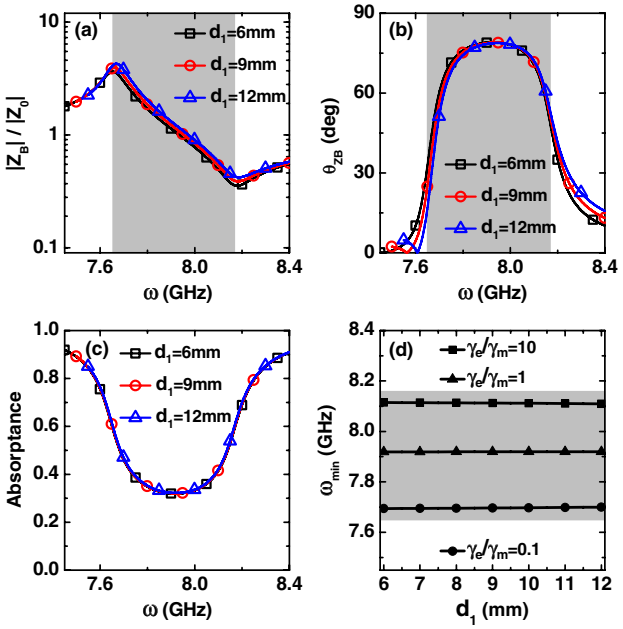

Fig. 8. (a) $|Z_B|$, (b) θ_{ZB}, and (c) absorptance versus ω under different d_1 for DPS/DNG PC structures with $d_1/d_2 = 1/2$ and $\gamma_e = \gamma_m = 0.001$ GHz. (d) $\omega_{\min}$ as a function of d_1 in PC structures with $d_1/d_2 = 1/2$.

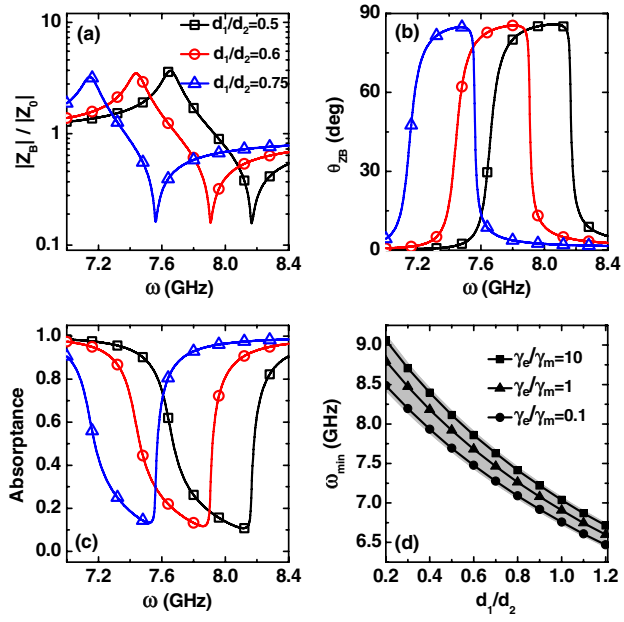

Fig. 9. (a) $|Z_B|$, (b) θ_{ZB}, and (c) absorptance versus ω under different d_1/d_2 for DPS/DNG PC structures with $d_1 = 6$ mm and $\gamma_e = 0.01$ GHz, $\gamma_m = 0.001$ GHz. The squares, circles, and triangles correspond to $d_2 = 12$, 10, and 8 mm, respectively. (d) $\omega_{\min}$ as a function of d_1/d_2 when $d_1 = 6$ mm.

conclude that the properties of the absorption loss within the zero-$\bar{n}$ gap are insensitive to the geometrical parameters of the photonic structures.

5. CONCLUSIONS

In summary, we have investigated the properties of the one-dimensional PCs consisting of alternating layers of air and lossy DNG metamaterials from the viewpoint of the Bloch impedance. We found that the absorption loss inside the zero-$\bar{n}$ gap is mainly determined by the phase angle rather than the complex modulus of the Bloch impedance. There exists a frequency which corresponds to the maximum phase angle of the Bloch impedance and minimum absorption loss inside the zero-$\bar{n}$ gap. Such a frequency is sensitive to the value of γ_e/γ_m of the DNG metamaterials. We also found that the changes of the geometrical parameters of the considered system do not influence the main characteristics of the Bloch impedance and the absorption loss.

ACKNOWLEDGMENTS

This work is supported by National Natural Science Foundation of China (grant 11274126), the Natural Science Foundation of Guangdong Province of China (grant 9151063101000040). This work is also supported by the U.S. Department of Energy (Basic Energy Science, Division of Materials Science and Engineering) under Contract No. DE-AC02-07CH11358.

REFERENCES

1. E. Yablonovitch, "Inhibited spontaneous emission in solid-state physics and electronics," Phys. Rev. Lett. **58**, 2059–2062 (1987).
2. S. John, "Strong localization of photons in certain disordered dielectric superlattices," Phys. Rev. Lett. **58**, 2486–2489 (1987).
3. K. Sakoda, *Optical Properties of Photonic Crystals* (Springer, 2001).
4. Y. Akahane, T. Asano, B.-S. Song, and S. Noda, "High-*Q* photonic nanocavity in a two-dimensional photonic crystal," Nature **425**, 944–947 (2003).
5. P. Tran, "Optical switching with a nonlinear photonic crystal: a numerical study," Opt. Lett. **21**, 1138–1140 (1996).
6. S. Noda, M. Fujita, and T. Asano, "Spontaneous-emission control by photonic crystals and nanocavities," Nat. Photonics **1**, 449–458 (2007).
7. V. G. Veselago, "The electrodynamics of substances with simultaneously negative values of ε and μ," Sov. Phys. Usp. **10**, 509–514 (1968).
8. D. R. Smith, W. J. Padilla, D. C. Vier, S. C. Nemat-Nasser, and S. Schultz, "Composite medium with simultaneously negative permeability and permittivity," Phys. Rev. Lett. **84**, 4184–4187 (2000).
9. R. A. Shelby, D. R. Smith, and S. Schultz, "Experimental verification of a negative index of refraction," Science **292**, 77–79 (2001).
10. J. Li, L. Zhou, C. T. Chan, and P. Sheng, "Photonic band gap from a stack of positive and negative index materials," Phys. Rev. Lett. **90**, 083901 (2003).
11. H. T. Jiang, H. Chen, H. Q. Li, Y. W. Zhang, and S. Y. Zhu, "Omnidirectional gap and defect mode of one-dimensional photonic crystals containing negative-index materials," Appl. Phys. Lett. **83**, 5386–5388 (2003).
12. Y. H. Chen, J. W. Dong, and H. Z. Wang, "Conditions of near-zero dispersion of defect modes in one-dimensional photonic crystals containing negative-index materials," J. Opt. Soc. Am. B **23**, 776–781 (2006).
13. H. Daninthe, S. Foteinopoulou, and C. M. Soukoulis, "Omnireflectance and enhanced resonant tunneling from multilayers containing left-handed materials," Photon. Nanostr. Fundam. Appl. **4**, 123–131 (2006).
14. V. M. Shalaev, "Optical negative-index metamaterials," Nat. Photonics **1**, 41–48 (2007).
15. C. M. Soukoulis, S. Linden, and M. Wegener, "Negative refractive index at optical wavelengths," Science **315**, 47–49 (2007).
16. C. M. Soukoulis and M. Wegener, "Past achievements and future challenges in the development of three-dimensional photonic metamaterials," Nat. Photonics **5**, 523–530 (2011).
17. A. Grbic and G. V. Eleftheriades, "Experimental verification of backward-wave radiation from a negative refractive index metamaterial," J. Appl. Phys. **92**, 5930–5935 (2002).
18. B. D. F. Casse, W. T. Lu, Y. J. Huang, E. Gultepe, L. Menon, and S. Sridhar, "Super-resolution imaging using a three-dimensional metamaterials nanolens," Appl. Phys. Lett. **96**, 023114 (2010).
19. D. S. Bethune, "Optical harmonic generation and mixing in multilayer media: analysis using optical transfer matrix techniques," J. Opt. Soc. Am. B **6**, 910–916 (1989).
20. B. Gralak, S. Enoch, and G. Tayeb, "Anomalous refractive properties of photonic crystals," J. Opt. Soc. Am. A **17**, 1012–1020 (2000).
21. Z. Y. Li and L. L. Lin, "Photonic band structures solved by a plane-wave-based transfer-matrix method," Phys. Rev. E **67**, 046607 (2003).
22. A. Yariv and P. Yeh, *Optical Waves in Crystal, Propagation and Control of Laser Radiation* (Wiley, 1984).
23. P. Markoš and C. M. Soukoulis, *Wave Propagation: From Electrons to Photonic crystals and Left-handed Materials* (Princeton, 2008).
24. D. M. Pozar, *Microwave Engineering* (Wiley, 1998).
25. R. Biswas, Z. Y. Li, and K. M. Ho, "Impedance of photonic crystals and photonic crystal waveguides," Appl. Phys. Lett. **84**, 1254–1256 (2004).
26. F. J. Lawrence, L. C. Botten, K. B. Dossou, C. M. de Sterke, and R. C. McPhedran, "Impedance of square and triangular lattice photonic crystals," Phys. Rev. A **80**, 023826 (2009).
27. S. Boscolo, M. Midrio, and T. F. Krauss, "Y junctions in photonic crystal channel waveguides: high transmission and impedance matching," Opt. Lett. **27**, 1001–1003 (2002).
28. Q. V. Tran, S. Combrié, P. Colman, and A. De Rossi, "Photonic crystal membrane waveguides with low insertion losses," Appl. Phys. Lett. **95**, 061105 (2009).